# One-Pot Synthesis of Fluorescent Carbon Nanoribbons, Nanoparticles, and Graphene by the Exfoliation of Graphite in Ionic Liquids

**Jiong Lu, Jia-xiang Yang, Junzhong Wang, Ailian Lim, Shuai Wang, and Kian Ping Loh***

Department of Chemistry, National University of Singapore, 3 Science Drive 3, Singapore 117543

**ABSTRACT** In this work we demonstrate a facile means to generate fluorescent carbon nanoribbons, nanoparticles, and graphene from graphite electrode using ionic liquid-assisted electrochemical exfoliation. A time-dependence study of products exfoliated from the graphite anode allows the reconstruction of the exfoliation mechanism based on the interplay of anodic oxidation and anion intercalation. We have developed strategies to control the distribution of the exfoliated products. In addition, the fluorescence of these carbon nanomaterials can be tuned from the visible to ultraviolet region by controlling the water content in the ionic liquid electrolyte.

**KEYWORDS:** carbon nanoribbons · carbon nanoparticles · graphene · electrochemistry · ionic liquids · fluorescent nanoparticles

Luminescent semiconductor quantum dots have been widely used in biology and medicine for biolabeling and bioimaging applications.[1] However, the known toxicity and potential environmental hazard of these inorganic nanomaterials limit their widespread use and *in vivo* applications in humans. Fluorescent carbon-based nanomaterals including nanotubes,[2,3] fullerenes,[4] and nanoparticles,[5,6] with their well-known biocompatibility, may be a more suitable alternative for *in vivo* biolabeling. Recently, zero-dimension fluorescent carbon nanoparticles with relatively high quantum yield have attracted intense interest. These carbon nanoparticles have been produced by the laser ablation of graphite,[5,6] by electrochemical route,[7,8] or by the chemical oxidation of candle soot.[9] Although the preparation methods are diverse, the basic mechanism involves the exfoliation of carbon from a graphitic source and its dissolution as particles. From the perspective of synthesis, it is desirable to identify a unified approach which can be applied for preparing a diverse range of carbon nanomaterials, that is, nanotubes, nanoribbons, graphene sheets, and nanoparticles. However, the development of facile and practical processing methods still remains a challenging issue. Herein, our search for a unifying approach in the diversity-oriented synthesis of carbon nanomaterials leads us to the use of ionic liquids for the electrochemical exfoliation of graphite.

Ionic liquids (ILs) have been proposed as "green" alternatives to conventional solvents[10,11] because of their unique properties like negligible vapor pressure, thermal stabilities, wide electrochemical potential window, low viscosity, good ion conductivity, and recyclability. These properties render ILs a very useful medium for liquid/liquid extraction, electrochemistry, chemical syntheses, and catalysis.[12,13] The high dielectric constant of ILs provides shielding for the stacking interactions caused by van der Waals interaction and helps to disperse these nanomaterials effectively. The marriage between ILs and carbon nanotubes forms a gel-like composite called "bucky gel".[14] These designer materials show great versatility for applications in capacitors, sensors, and actuators. Recently, Liu *et al*. demonstrated the exfoliation of graphene sheets from graphite anode in ionic liquid.[15] This approach is promising because generating exfoliated graphene sheets directly from graphite will circumvent the problem of low conductivity faced by graphene films chemically reduced from graphene oxide derivatives. Graphene oxide-derived materials possess a high density of defects which have deleterious effects on the carrier mobility.[16]

However the detailed mechanism of the exfoliation was not investigated in Liu's work. Water is often the main impurity in the ILs, and we suspect that water plays a very important role in controlling the shape

*Address correspondence to chmlohkp@nus.edu.sg.

Received for review May 26, 2009 and accepted July 27, 2009.

**Published online August 5, 2009.**
10.1021/nn900546b CCC: $40.75

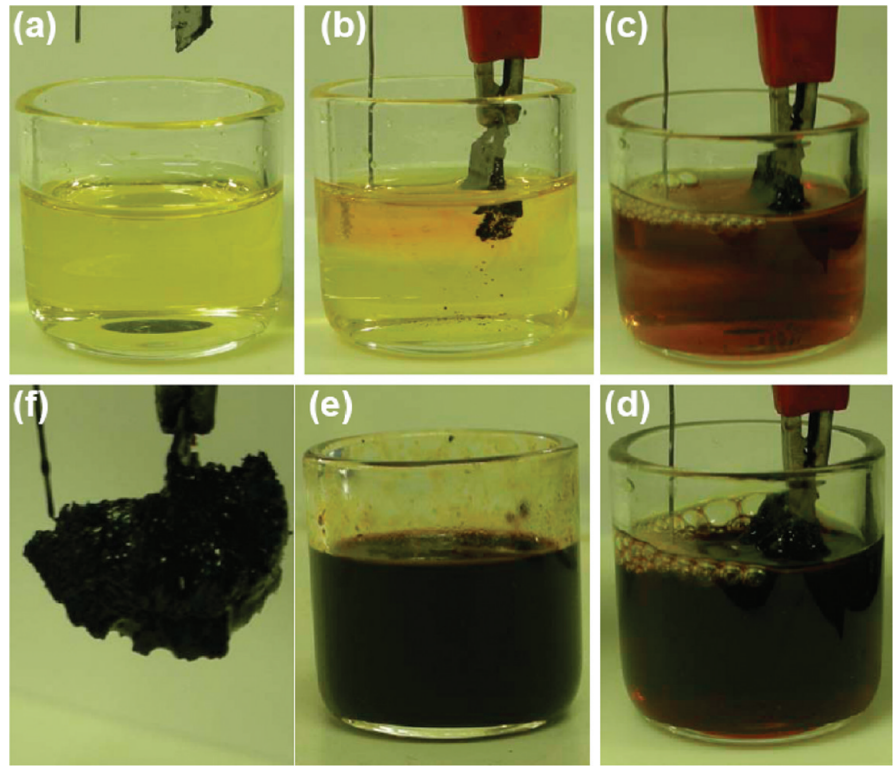


**Figure 1. Time evolution of IL electrolyte and highly oriented pyrolytic graphite (HOPG) anode during exfoliation in 60 wt % water/[BMIm][$BF_4$] electrolyte. Stages of I, II, and III are shown correspondingly in panels b,c, and d. Heavily expanded HOPG is obtained in panel f.**

of the exfoliated products. In the course of investigating the role of water in the exfoliation mechanism, we discovered that a diverse range of nanostructured carbon materials can be generated by controlling the ratio of water to ILs in the electrolyte. In addition to the graphene sheets, water-soluble fluorescent carbon nanoparticles and nanoribbons could be generated during the exfoliation. By tuning the water content and type of counterions in the ILs, the fluorescence, as well as the distribution of the nanomaterial, can be tuned. This method of nanomaterial preparation is highly versatile and industrially scalable.

## RESULTS AND DISCUSSION

According to the proposed mechanism by Liu,[15] the positively charged imidazolium ion is reduced at the cathode to form the imidazolium free radical[17] which can insert into the $\pi$ bonds of the graphene plane. At the fundamental level, there are several questionable aspects about the radical-insertion mechanism proposed by Liu,[15] especially when the ILs are mixed with water at 1:1 ratio and where an operational voltage as high as 15 V is applied. When we carried out the experiments using twin graphite electrodes, we observed that the exfoliation of the graphite occurs only at the anode and the graphite cathode is intact throughout the course of the experiment. If the imidazolium radicals were generated at the cathode, the cathode should be attacked by the radicals and became exfoliated, but this did not happen. Typically, the voltages applied in these electrochemical experiments exceeded the rather narrow electrochemical potential window of water. This results inevitably in the generation of hydroxyl and oxygen radicals from the dissociation of water. Even at 10% water content, sufficient quantities of these radicals can attack the anode to result in its sacrificial corrosion during the electrochemical reactions. Intrigued by these questions, we used a water-miscible ionic liquid 1-butyl-3-methylimidazolium tetrafluoroborate [BMIm][$BF_4$] and mixed it with water at different fractions to be used as electrolyte for the electrochemical exfoliation of graphite. The viscosity and conductivity of the ILs is affected significantly by the presence of water, its major impurity. In an IL, there is a complex interplay of forces such as Coulombic, van der Waals, hydrogen bonding, and $\pi-\pi$ interactions which control its solvation and internal order. The addition of water within the ionic liquids disrupts the internal organization and modifies the liquid structure by forming a new hydrogen-bonded network. This decreases the cohesive energy and lowers the viscosity of the ILs.[15,18]

The effect of water on the electrochemical properties of ILs can be investigated using cyclic voltammetry (CV) as shown in Supporting Information Figure-S1. It is observed that the electrochemical potential window of the IL/water mixture narrows with the addition of water, decreasing dramatically from 4.2 V at 0 wt % $H_2O$ to 2.8 V in 10 wt % $H_2O$ and finally to 2.2 V at 90 wt % $H_2O$.

Parallel with the narrowing of the electrochemical potential window as well as the lowering of the electrolyte resistance with increasing water content, the onset of exfoliation is observed to occur at lower activation voltages. For example, in 90 wt % water/[BMIm][$BF_4$] electrolyte, the exfoliation can be activated at 1.5−2.0 V. This potential has to be increased to 2.5−3 V in the case of 60 wt % and 7−8 V in the case of 10 wt %. We can infer that the trend of decreasing activation voltages with increasing water content is correlated to the smaller overpotential required for the electrochemical oxidation of water. As such, hydroxyl radicals released from the oxidation of water may play an important role in the first stage of exfoliation.

Three stages in the electrochemical exfoliation, which reflect the time evolution in the dynamic process of electrochemical oxidation, intercalation, and expansion of the graphite anode, are typified by the sequential images of the electrochemical cell shown in Figure 1. In stage **I**, there is an induction period before visible signs of exfoliation can be detected. The color of the electrolyte changed from colorless to yellow and then dark brown. In stage **II**, a visible expansion of the graphite anode can be seen. In stage **III**, the expanded flakes peel off from the anodes and form the black slurry with the electrolyte. The intensity of the coloration varied for ILs with different water content. A more concentrated IL electrolyte will develop a dark coloration faster, as opposed to light coloration for a more diluted IL electrolyte. Some precipitation could be found at the bottom in stages **II** and **III.** The demarcation of these stages is significant because different products are obtained from the graphite anode when the electrolyte assumed a specific color. The products from the different stages were extracted and purified to have their structure analyzed by transmission electron microscopy (TEM).

In stage **I**, 8−10 nm sized, hexagonal-shaped, water-soluble, and fluorescent carbon nanocrystals are produced, as shown in Figure 2a. The HR-TEM image in Figure 2b reveals that these nanocrystals have a lattice spacing of 0.21−0.25 nm which is comparable to the (100) facet of graphite. In stage **II**, the predominant products are fluorescent nanoribbons of 10 nm × (60 ± 20) nm size with flat rectangular edges, as well as some graphene sheets. The carbon nanoribbons have a lattice distance of 0.34 nm that corresponds to the (002) plane of graphite, as shown in Figure 2c,d. The TEM images of ultrathin graphene sheets (200 nm × 500 nm) are presented in Figure 2e,f.

The mechanism of the exfoliation could be deduced from the sequences of the appearance of the exfoliated products, which we further confirmed by studying the effects on the exfoliated products by changing the counterion and magnitude of voltages applied. The time evolution of the exfoliation process is illustrated in Scheme 1, and summarized as follows:

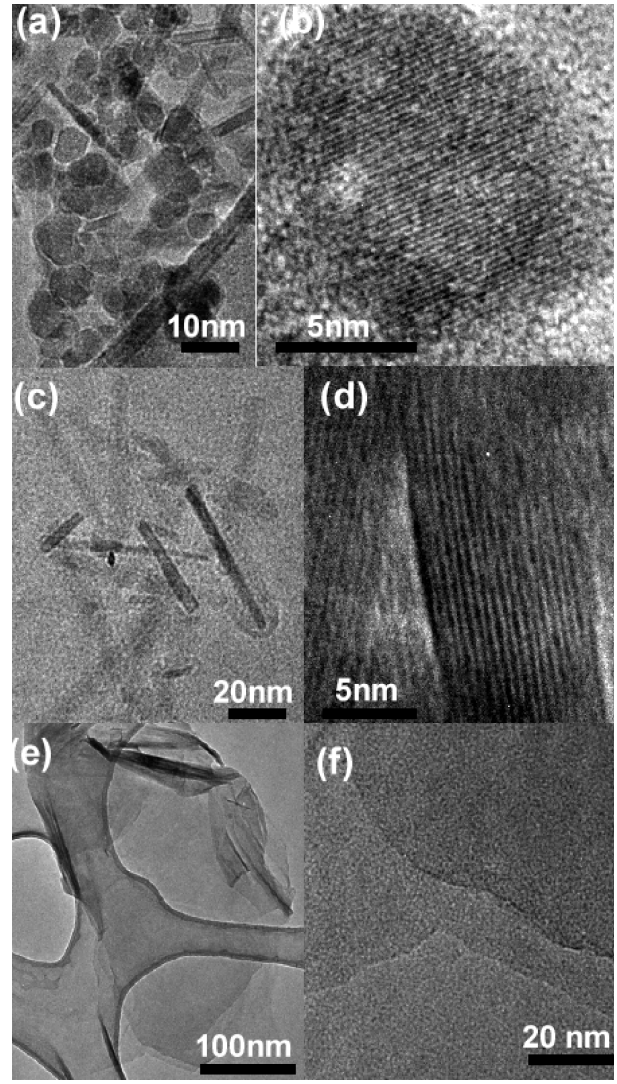


**Figure 2. TEM images of carbon nanoparticles (a,b), carbon nanoribbons (c,d), and graphene sheets (e,f) produced in the one-pot electrochemical exfoliation.**

(1) Anodic oxidation of water produced hydroxyl and oxygen radicals.

$$\text{anode: } H_2O \xrightarrow{-e} \cdot OH + H^+ \xrightarrow{-e} \cdot O + H^+$$

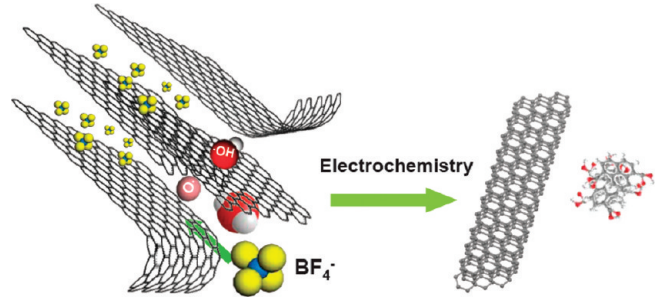


**Scheme 1. Illustration of the exfoliation process showing the attack of the graphite edge planes by hydroxyl and oxygen radicals, which facilitate the intercalation of $BF_4^-$ anion. The dissolution of hydroxylated carbon nanoparticles gives rise to the fluorescent carbon nanoparticles. Oxidative cleavage of the expanded graphite produces graphene nanoribbons.**

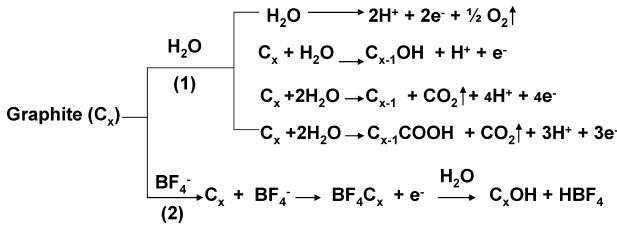


**Scheme 2. The interplay of (1) anodic oxidation of water as well as (2) intercalation of $BF_4^-$ anions controlled the shape of the exfoliated products.**

The hydroxylation or oxidation of graphite by these radicals results in the dissolution of fluorescent carbon nanocrystals from the anode. The corrosion process occurs initially at edge sites, grain boundaries, or defect sites and takes place before the expansion of the graphite electrode.

(2) The oxidation of the edge planes opens up the edge sheets, facilitating intercalation by the anionic $BF_4^-$, which leads to the depolarization and expansion of the graphite anode[19,20]

(3) Oxidative cleavage of the expanded graphene sheets generates graphene nanoribbons.

(4) Some expanded sheets precipitate as graphene sheets.

The electrochemical reactions involve the interplay of the $BF_4^-$ anion from the ILs, as well as water. The equations[21] are represented as seen in Scheme 2

Tuning the composition of the IL/$H_2O$ affects the exfoliation mechanism and changes the shape and size distribution of the exfoliated products. $BF_4^-$ ion has a higher oxidation potential than water,[22] thus water will be sacrificially oxidized at the anode to generate hydroxyl and oxygen radicals. $BF_4^-$ plays the role of intercalator in the graphite planes. Two limiting cases can be highlighted:

(1) Increasing the IL/water ratio increases the proportion of $BF_4^-$ ion to water; this facilitates the intercalation process by $BF_4^-$ and the expansion of graphene anode. The heavily expanded graphite is more susceptible to oxidative cleavage to form nanoribbons.

(2) Increasing the water/IL content results in larger concentration of OH and O radicals; these species oxidize the graphite anode and results in its dissolution as hydroxylated carbon particles.

According to the above mechanism, the O and OH radicals derived from the anodic oxidation of water plays the role of an electrochemical "scissors" in its oxidative cleavage reaction. An "unzipping" mechanism has been invoked to explain the cutting of carbon nanotubes and graphene, where the strain induced by the formation of oxygenated groups such as epoxy encouraged further oxidative attack and cleavage.[23]

The interplay of water and ILs anion in controlling the types of products generated in the exfoliation can be illustrated by changing the counterion in the ILs to one that has a lower oxidation potential than water, such that this counterion becomes preferentially anodically oxidized. In this case, even in water-rich IL, the products are predominantly influenced by the action of the IL anion. The IL 1-methyl-3-butylimidazolium chloride ([BMIm]Cl) has the same cation but a different anion in the form of $Cl^-$. At 90 wt % water content, the major products obtained in the exfoliation are now carbon nanoribbons, as opposed to carbon nanocrystals when $BF_4^-$ is the anion. The products obtained were also less oxidized. This is due to the lower overpotential for the oxidation of $Cl^-$. In ionic liquid, the two-step oxidation of $Cl^-$ anion results in the formation of $Cl_3$ anion.[13] The $Cl_3$ anion plays the role of the anion intercalator, which leads to the ready expansion of the graphite electrode and its oxidative cleavage. The TEM images of carbon nanoribbons are shown in Figure 3. It can be seen that the nanoribbons are surrounded by an adventitious layer of ILs, these could be readily removed by ion exchange. The HR-TEM image in Figure 3b reveals that the carbon nanoribbons have similar lattice constant as that of graphite.

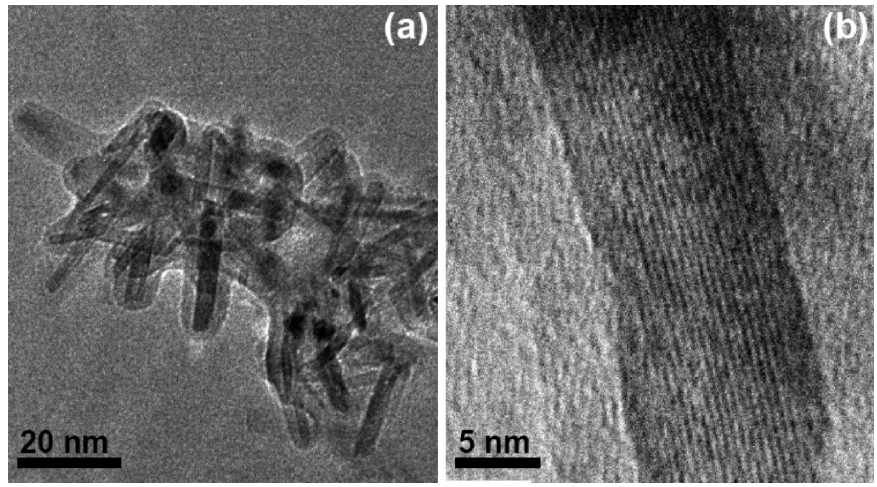


**Figure 3. TEM images of carbon nanoribbons produced by electrochemical exfoliation using 90 wt % water/[BMIm]Cl electrolyte.**

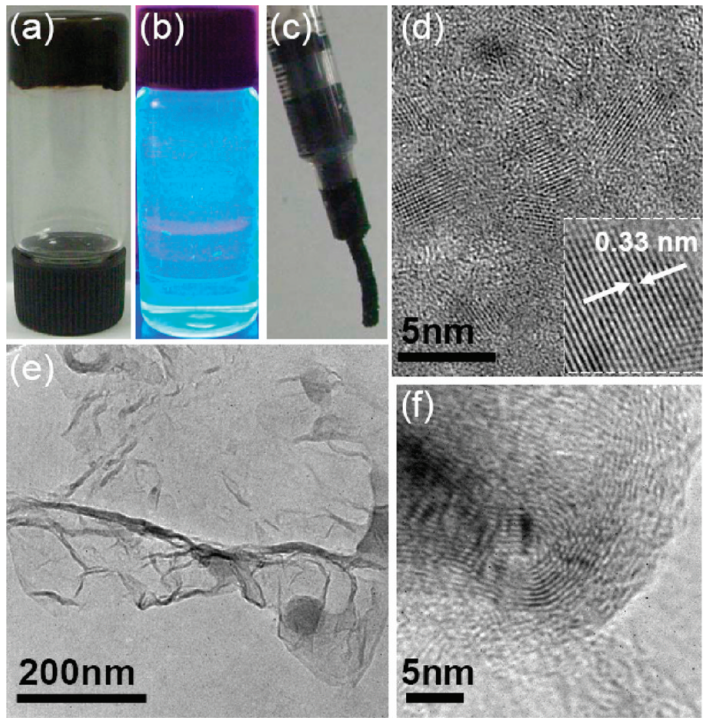


**Figure 4. "Bucky" gel produced by electrochemical exfoliation in pure ionic liquid [BMIm][$BF_4$]. (a) The supernatant contains ILs-functionalized carbon nanoparticle (ILCN) that emits in the blue, as shown in panel b. (c) Extrusion of the bucky gel; (d and f) TEM images showing ILCN found in the supernatant; (e) carbon nanosheets found in bucky gel.**

The exfoliation experiment was also carried out in pure ionic liquid [BMIm][$BF_4$] which had been extensively bubbled with argon to remove dissolved oxygen. Higher activation voltages of 6−8 V are needed to initiate the exfoliation. Similar to the exfoliation process as shown in Figure 1, the color of electrolyte changes from light yellow, brown, dark brown, to black. The electrolyte becomes highly viscous after some time. A "bucky gel" can be recovered from the bottom of the tube after the mixture is centrifuged at 15000 rmp to remove excess ionic liquid, as shown in Figure 4a. These gels can be extruded to form a paste useful

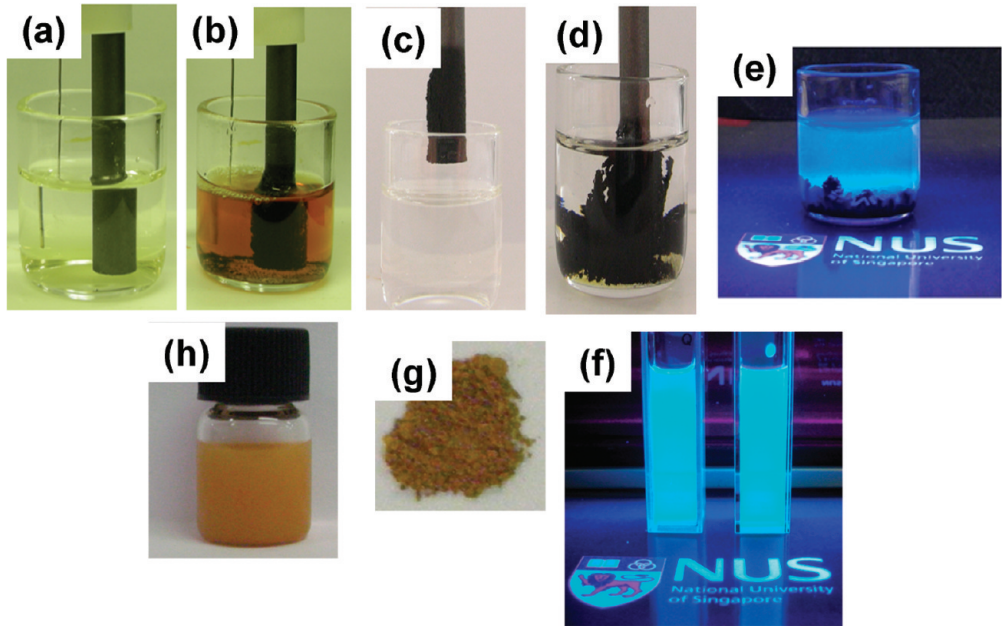


**Figure 5. Graphite rod exfoliated in IL-$BF_4$/water (40:60) mixture solution: (a,b) color change of the electrolyte solution with the corrosion of the graphite rod; (c) the expanded graphite rod is immersed into DMF after washing with acetone; (d) the expanded portion of the anodic graphite rod is exfoliated in DMF; (e and f) the supernatant solution emits blue fluorescence upon irradiation with 254 nm UV light; (g) bulk quantities of carbon nanopariticles (6−8 nm) can be recovered; (h) carbon nanoparticles can be dispersed in water.**

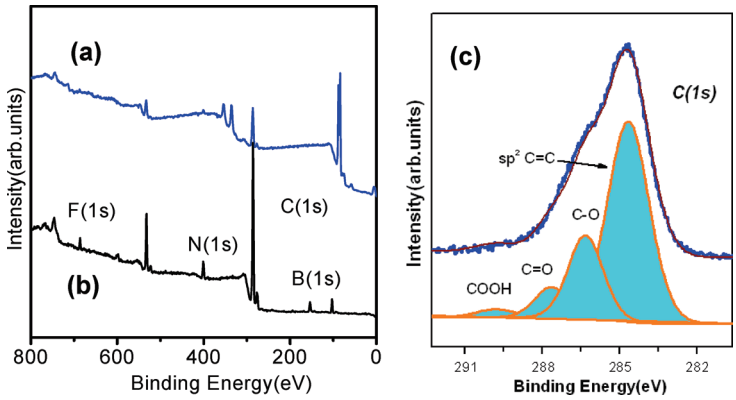


**Figure 6. XPS spectra of products generated by electrochemical exfoliation in electrolyte with water content (a) more than 10 wt %; (b) less than 10 wt %; (c) C 1s spectrum of oxidized carbon nanomaterials.**

for the modification of electrodes to enhance conductivity and sensing (Figure 4c). Figure 4 panels d and e show the nanoparticles and graphene sheets isolated from the bucky gel. X-ray photoelectron spectroscopy (XPS) analysis reveals that the graphene sheets are functionalized with the ILs; the latter may interact with the π-electronic surface of the graphene sheets by cation−π and/or π−π interactions. The supernatant is found to contain IL-functionalized blue-emitting materials, as shown in Figure 4b.

Fluorescent nanomaterials are abundant in the supernatant containing the soluble exfoliates. Figure 5 illustrate the ease of generation and recovery of these fluorescent nanomaterials. We began by dipping a graphite rod into the ionic liquid mixture together with a Pt counter electrode and applied DC voltage for 240 min. The pictures show the dissolution of carbon nanomaterials into the ILs electrolyte, and the expansion of the graphite rod. The expanded graphite rod can be removed from the ILs and dip into pure DMF for 2 min, and upon illumination with UV light, strong fluorescence from the DMF solution can be seen. TEM analysis of the solution finds abundant nanoribbons and nanoparticles in the solution and separation of these products reveals that both materials are fluorescent (refer optical characterization section). Very importantly, bulk quantities of fluorescent carbon nanomaterials can be recovered by this method. A rough estimate revealed a yield of close to 80% weight percent transformation from graphite rod into fluorescent carbon materials.

X-ray photoelectron spectroscopy (XPS) was used to monitor the composition of the exfoliated products after rigorous purification of the products and multiple washing. As shown in the XPS survey scan in Figure 6a, no trace of IL can be detected in the exfoliated nanosheets, nanoparticles, or nanoribbons when the electrolyte contains less than 10% by weight of water. The absence of peaks corresponding to B, F, and N, which will be expected if the IL is linked to the exfoliated products, proves that the intercalated $BF_4^-$ anions are readily displaced during washing. The main modification appears to be oxidation. With increasing water content in the IL, XPS analysis reveals the growth of a chemically shifted component attributable to C−O, C═O, COOH as shown in Figure 6c. This proves that the oxidative dissolution of the graphite electrode is related to the presence of water. The oxidation imparts water solubility on the nanoribbons and nanoparticles, and also influences the optical properties of the exfoliated nanomaterials, as shown later.

Figure 7 shows the XPS C 1s of the various exfoliated carbon nanomaterials generated in ILs mixed with water at different weight percentages. It is very clear that higher water content results in a greater degree of oxidation. For ILs mixed with the same amount of water but differing in the type of counterions, for example, $BF_4^-$ *versus* $^-Cl_3$, it is found that using $Cl_3$ anion results in a lesser degree of oxidation of the carbon, due to the lower oxidation potential of $Cl^-$ to form $Cl_3$ anion compared to water. Thus the anodic oxidation of water can be suppressed by using a sacrificial anion which can undergo preferential oxidation.

The functionalization of the graphene sheets by ILs occurred only when a concentrated IL with less than 10% water was used as the electrolyte. The presence of the imidazolium moiety as well as the $BF_4^-$ counterion can be seen clearly in the XPS survey scan in Figure 6b as well as the high resolution spectra in Figure 8. A well-defined peak at 400.2 eV can be assigned to the N 1s of the imidazolium ion. The presence of B 1s peak at 193.3 eV and F 1s at 686.5 eV supports the presence of the $BF_4^-$ anion. The origin of these peaks is due to a tenaciously bound IL coat around the surface of graphene sheets.

Raman spectroscopy was applied to evaluate the crystalline quality of the exfoliated materials. The Raman spectrum in Figure 9 was collected from exfoliated

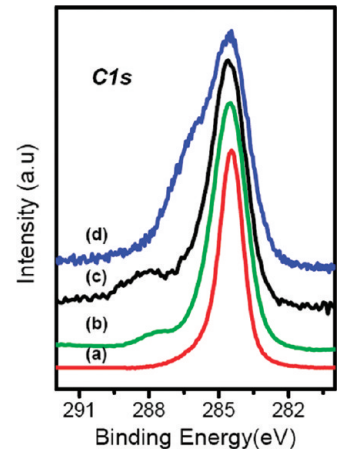


**Figure 7. XPS C 1s spectra of (a) graphene precipitates and soluble graphene produced by electrochemical exfoliation in (b) 90 wt % water in [BMIm]Cl, (c) 60 wt % water in [BMIm][$BF_4$], (d) 90 wt % water in [BMIm][$BF_4$].**

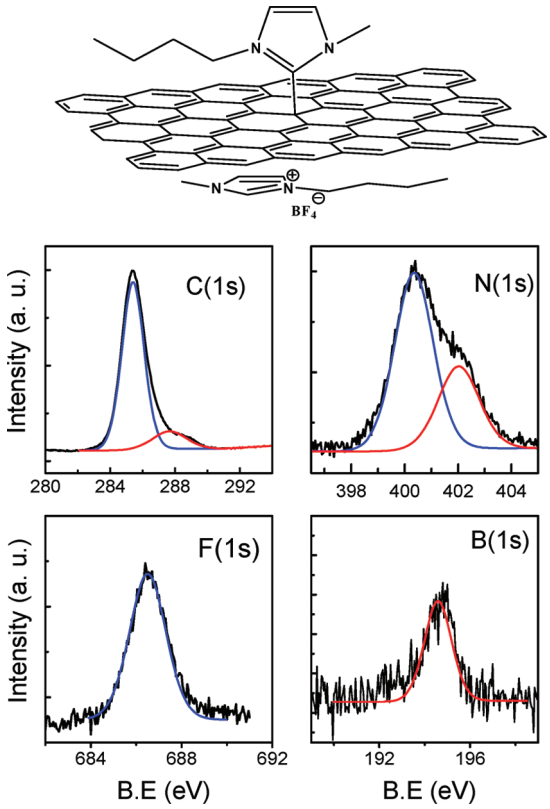


**Figure 8. XPS spectra of graphene sheets exfoliated in concentrated ILs with less than 10 wt % water. The presence of N 1s, B 1s, and F 1s evidenced the functionalization of the graphene sheets by ILs. The top picture shows various possibilities of attachment of ILs to graphene, *via* covalent or noncovalent interactions.**

graphene sheets which were spin-coated on silicon oxide-coated silicon wafers. The major Raman features, common to all chemically processed graphene samples, are the D band at 1361 $cm^{-1}$, G band at 1580 $cm^{-1}$, and 2D band at 2683 $cm^{-1}$.[24,25] The D band is related to the presence of $sp^3$ defects. The G band is related to the in-plane vibration of $sp^2$ carbon atoms which is a doubly degenerate (TO and LO) phonon mode ($E_{2g}$ symmetry) at the Brillouin zone center. The presence of a sharp and symmetric 2D band which originates from a

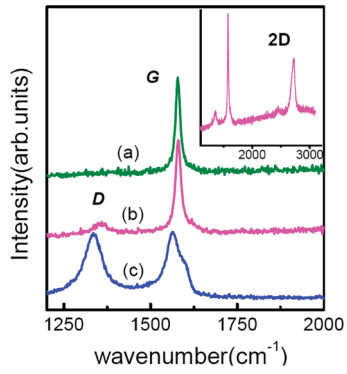


**Figure 9. Raman spectra of (a) graphene precipitates; (b) ILs-functionalized graphene in DMF; (c) oxidized carbon nanoribbons and carbon nanoparticles. The inset shows the sharp 2D peak corresponding to panel b.**

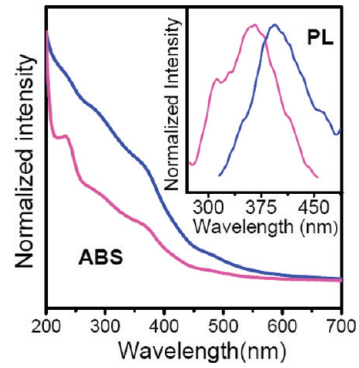


**Figure 10. UV−vis absorption and fluorescence spectra (inset figure) obtained for 8−10 nm carbon nanoparticles (red curve) and carbon nanoribbons (blue curve). The emission spectrum was obtained using 260 nm excitation.**

two phonon double resonance Raman process is used as a fingerprint to identify single or bilayer graphene. The Raman data proves that the thin imidazolium-decorated graphene sheets have significantly lower density of defects compared to exfoliated nanomaterials based on its relatively weak D band and its sharp 2D band (fwhm 70 $cm^{-1}$). In contrast, the exfoliated carbon nanoribbons and nanocrystals have a high density of defects as judged from the stronger D peak in the Raman spectrum in Figure 9c. The exfoliation of these products involves the oxidation process at the graphite anode; the decoration of the surfaces of these materials by oxygen groups gives rise to surface defects. As the D band is related to edge defects,[26] the relative increase of the D band in the exfoliated carbon nanoribbons and nanocrystals can also be explained by the increased proportions of surface defects as well as the larger surface-to-volume ratio of these materials.

The UV−vis absorption and fluorescence spectra of the carbon nanoribbons (10 nm × (60 ± 20) nm) and carbon nanoparticles (8−10 nm) are shown in Figure 10. The PL of carbon nanoribbons is distinct from that of the carbon nanoparticles (Figure 10 inset). The PL peak is centered at 395 nm (3.13 eV), which is red-shifted from that of the carbon nanoparticles at 364 nm (3.40 eV). The PL spectra of the carbon nanoparticles are generally broad and dependent on excitation wavelengths, which may be due to the size heterogeneity and distribution of different emissive sites on the carbon nanoparticles.

Figure 11 shows that both the UV adsorption and PL peaks shift to short wavelength as the water content in the IL increases. In terms of the size of the particle, this trend is opposite to what one would expect from quantum confinement effects. In pure ILs, the carbon nanoparticles are 2−4 nm in diameter and emit at 440 nm (Figure 4d). In water-rich ILs, the size of the carbon nanoparticles is larger (8−10 nm), and the emission is centered at 364 nm (3.40 eV). This indicates that chemical composition, rather than size, is the major factor controlling the emission. XPS analysis reveals that

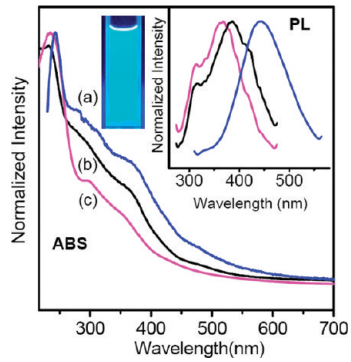


**Figure 11. UV adsorption and PL peak of carbon nanoparticles electrochemical exfoliated using IL electrolytes containing different water content. The emission spectra were excited using 260 nm light: (a, blue curve) 10 wt % water; (b, black curve) 60 wt % water; (c, pink curve) 90 wt % water. A blue shift of the emission is apparent with higher wt % of water in the electrolyte.**

exfoliated particles obtained under water-rich conditions are oxidized, hence these particles resemble graphene oxide. It can be expected that oxidation produced a disruption of the $\pi$ network and opened a direct electronic band gap, and that the size of these gaps will increase with the degree of oxidation.[27,28]

The exfoliated carbon nanoparticles produced in water-poor ILs (water content $<$10%) have strong photoluminescence with a quantum yield of 2.8−5.2%. These carbon nanoparticles are functionalized by the ILs. The emission window is wide and extends from 400 to 600 nm. (Supporting Information Figure S2). The photoluminescence from these carbon nanoparticles may be attributed to the presence of surface energy traps that become emissive upon stabilization as a result of the surface passivation by ILs. The functionalization by IL moieties improves the dispersion of the nanoparticles and diminishes the quenching effects due to interparticle interaction.[29]

## CONCLUSIONS

We have developed a unified one-pot electrochemistry method to prepare fluorescent carbon nanoribbons, nanoparticles, and graphene sheets from the exfoliation graphite electrode. The mechanism of the exfoliation is due to a complex interplay of anodic oxidation of water and anionic intercalation from the ionic liquid. Using ILs with high water content ($>$10% water) as the electrolyte, water-soluble, oxidized carbon nanomaterials are generated. In the case of electrolyte using concentrated ILs ($<$10% water), IL-functionalized carbon nanomaterials are generated instead. For the first time, we demonstrated that carbon nanoribbons could be produced directly from graphite by the concerted action of anionic intercalation and oxidative cleavage. The chemical composition and surface passivation of the exfoliated carbon nanoparticles can be controlled by changing the water/IL ratio in the electrolyte, thus allowing the fluorescence from the exfoliated nanoparticles to be tuned from the ultraviolet to visible regions. It is clear that this method allows upward scalability in terms of the production of bulk quantities of fluorescent and biocompatible carbon nanomaterials which could be applied in biological labeling and imaging.

## EXPERIMENTAL SECTION

**Methods.** All other chemicals were purchased from Sigma-Aldrich and used directly without further purification. High-purity graphite rods and highly oriented pyrolytic graphite (HOPG) (1 cm × 1 cm × 1 mm) were purchased from the SPI Co. Ltd. The graphite rod and HOPG were inserted as anode into the ionic liquid (IL)/water solution, placed parallel to the Pt wire as counter-electrode with a separation of 2 cm. In our experiment, the ionic liquid 1-methyl-3-butylimidazolium tetrafluoroborate (or 1-methyl-3-butylimidazolium chloride) was mixed with water with different ratios. Static potentials of 1.5−15 V were applied to the two electrodes using a DC power supply. The exfoliation products were washed with water and ethanol until the pH was neutral and the products were separated by filter and ultracentrifugation at 15000 rmp (23400*g*) at 20 °C.

**Characterization.** Transmission electron microscopy (TEM) measurements were conducted with a JEOL JEM-3010 microscope at an acceleration voltage of 300 kV. SEM images were obtained on JEOL 6701 FESEM (field emission scanning electron microscopy) at 30 kV. X-ray photoelectron spectroscopy (XPS) was performed with the Phobios 100 electron analyzer equipped with five channeltrons, using an unmonochromated Mg Kα X-ray source (1253.6 eV). The UV−vis absorption and photoluminescence spectra were recorded on a Shimadzu UV 2450PC spectrophotometer and Perkin-Elmer LS 55 luminescence spectrometer, respectively. The Raman spectra were recorded by a Renishaw inVis Microscope Raman spectrometer with an argon-ion laser at an excitation wavelength of 514 nm. All the measurements were taken at room temperature without special mention.

*Acknowledgment.* We thank NRF-CRP grant "R-143-000-360-281: Graphene Related Materials and Devices."

*Supporting Information Available:* Cyclic voltammograms and fluorescence emission data. This material is available free of charge *via* the Internet at http://pubs.acs.org.

## REFERENCES AND NOTES

1. Michalet, X.; Pinaud, F. F.; Bentolila, L. A.; Tsay, J. M.; Doose, S.; Li, J. J.; Sundaresan, G.; Wu, A. M.; Gambhir, S. S.; Weiss, S. Quantum Dots for Live Cells, *in Vivo* Imaging, and Diagnostics. *Science* **2005**, *307*, 538–544.
2. O'Connell, M. J.; Bachilo, S. M.; Huffman, C. B.; Moore, V. C.; Strano, M. S.; Haroz, E. H.; Rialon, K. L.; Boul, P. J.; Noon, W. H.; Kittrell, C.; *et al.* Band Gap Fluorescence from Individual Single-Walled Carbon Nanotubes. *Science* **2002**, *297*, 593–596.
3. Riggs, J. E.; Guo, Z.; Carroll, L. D.; Sun, Y. P. Strong. Luminescence of Solubilized Carbon Nanotubes. *J. Am. Chem. Soc.* **2000**, *122*, 5879–5880.
4. Schick, G.; Levitus, M.; Kvetko, L.; Johnson, B. A.; Lamparth, I.; Lunkwitz, R.; Ma, B.; Khan, S. I.; Garcia-Garibay, M. A.; Rubin, Y. Unusual Luminescence of Hexapyrrolidine Derivatives of $C_{60}$ with Th and Novel D3-Symmetry. *J. Am. Chem. Soc.* **1999**, *121*, 3246–3247.
5. Sun, Y. P.; Zhou, B.; Lin, Y.; Wang, W.; Fernando, K. A.; Pathak, P.; Meziani, M. J.; Harruff, B. A.; Wang, X.; Wang, H.; *et al.* Quantum-Sized Carbon Dots for Bright and Colorful Photoluminescence. *J. Am. Chem. Soc.* **2006**, *128*, 7756–7757.

6. Hu, S. L.; Niu, K. Y.; Sun, J.; Yang, J.; Zhao, N. Q.; Du, X. W. One-Step Synthesis of Fluorescent Carbon Nanoparticles by Laser Irradiation. *J. Mater. Chem.* **2009**, *19*, 484–488.
7. Zhou, J.; Booker, C.; Li, R.; Zhou, X.; Sham, T. K.; Sun, X.; Ding, Z. An Electrochemical Avenue to Blue Luminescent Nanocrystals from Multiwalled Carbon Nanotubes (MWCNTs). *J. Am. Chem. Soc.* **2007**, *129*, 744–745.
8. Zheng, L.; Chi, Y.; Dong, Y.; Lin, J.; Wang, B. Electrochemiluminescence of Water-Soluble Carbon Nanocrystals Released Electrochemically from Graphite. *J. Am. Chem. Soc.* **2009**, *131*, 4564–4565.
9. Liu, H.; Ye, T; Mao, C. Fluorescent Carbon Nanoparticles Derived from Candle Soot. *Angew. Chem., Int. Ed.* **2007**, *46*, 6473–6475.
10. Hardacre, C.; Holbrey, J. D.; Nieuwenhuyzen, M.; Youngs, T. G. A. Structure and Solvation in Ionic Liquids. *Acc. Chem. Res.* **2007**, *40*, 1146–1155.
11. Welton, T. Room-Temperature Ionic Liquids. Solvents for Synthesis and Catalysis. *Chem. Rev.* **1999**, *99*, 2071–2083.
12. Gutowski, K. E.; Broker, G. A.; Willauer, H. D.; Huddleston, J. G.; Swatloski, R. P.; Holbrey, J. D.; Rogers, R. D. Controlling the Aqueous Miscibility of Ionic Liquids: Aqueous Biphasic Systems of Water-Miscible Ionic Liquids and Water-Structuring Salts for Recycle, Metathesis, and Separations. *J. Am. Chem. Soc.* **2003**, *125*, 6632.
13. Hapiot, P.; Lagrost, C. Electrochemical Reactivity in Room-Temperature Ionic Liquids. *Chem. Rev.* **2008**, *108*, 2238–2264.
14. Fukushima, T.; Kosaka, A.; Ishimura, Y.; Yamamoto, T.; Takigawa, T.; Ishii, N.; Aida, T. Molecular Ordering of Organic Molten Salts Triggered by Single-Walled Carbon Nanotubes. *Science* **2003**, *300*, 2072–2074.
15. Liu, N.; Luo, F.; Wu, H.; Liu, Y.; Zhang, C.; Chen, J. One-Step Ionic-Liquid-Assisted Electrochemical Synthesis of Ionic-Liquid-Functionalized Graphene Sheets Directly from Graphite. *Adv. Funct. Mater.* **2008**, *18*, 1518–1525.
16. Lotya, M.; Hernandez, Y.; King, P. J.; Smith, R. J.; Nicolosi, V.; Karlsson, L. S.; Blighe, F. M.; De, S.; Wang, Z.; McGovern, I. T.; *et al*. Liquid Phase Production of Graphene by Exfoliation of Graphite in Surfactant/Water Solutions. *J. Am. Chem. Soc.* **2009**, *131*, 3611–3620.
17. Xiao, L.; Johnson, K. E. Electrochemistry of 1-Butyl-3-methyl-1H-imidazolium Tetrafluoroborate Ionic Liquid. *J. Electrochem. Soc.* **2003**, *150*, E307−E311.
18. Rubero-Rivera, S.; Baldelli, S. Influence of Water on the Surface of Hydrophilic and Hydrophobic Room-Temperature Ionic Liquids. *J. Am. Chem. Soc.* **2004**, *126*, 11788–11789.
19. Seela, J. A.; Dahn, J. R. Electrochemical Intercalation of $PF_6$ into Graphite. *J. Electrochem. Soc.* **2000**, *147*, 892–898.
20. Katinaonkul, W.; Lerner, M. M. Graphite Intercalation Compounds with Large Fluoroanions. *J. Fluorine Chem.* **2007**, *128*, 332–335.
21. Zimmer, E.; Krohn, H.; Beck, F. Corrosion of Graphite Intercalation Compounds. *Electrochim. Acta* **1986**, *31*, 371–376.
22. De Souza, R. F.; Padilha, J. C.; Conçalves, R. S.; Rault-Berthelot, J. Dialkylimidazolium Ionic Liquids as Electrolytes for Hydrogen Production from Water Electrolysis. *Electrochem. Commun.* **2006**, *8*, 211–216.
23. Li, J. L.; Kudin, K. N.; McAllister, M. J.; Prud'homme, R. K.; Aksay, I. A.; Car, R. Oxygen-Driven Unzipping of Graphitic Materials. *Phy. Rev. Lett.* **2006**, *96*, 176101.
24. Gupta, A. K.; Russin, T. J.; Gutiérrez, H. R.; Eklund, P. C. Probing Graphene Edges *via* Raman Scattering. *ACS Nano* **2009**, *3*, 45–52.
25. Ni, Z. H.; Yu, T.; Luo, Z. Q.; Wang, Y. Y.; Liu, L.; Wong, C. P.; Miao, J.; Huang, W.; Shen, Z. X. Probing Charged Impurities in Suspended Graphene Using Raman Spectroscopy. *ACS Nano* **2009**, *3*, 569–574.
26. Casiraghi, C.; Hartschuh, A.; Qian, H.; Piscanec, S.; Georgi, C.; Fasoli, A.; Novoselvo, K. S.; Basko, D. M.; Ferrari, A. C. Raman Spectroscopy of Graphene Edges. *Nano Lett.* **2009**, *9*, 1433–1441.
27. Luo, Z.; Vora, P. M.; Mele, E. J.; Johnson, A. T. C.; Kikkawa, J. M. Photoluminescence and Band Gap Modulation in Graphene Oxide. *Appl. Phys. Lett.* **2009**, *94*, 111909.
28. Mkhoyan, K. A.; Contryman, A. W.; Silcox, J.; Stewart, D. A.; Eda, G.; Mattevi, C.; Miller, S.; Chhowalla, M. Atomic and Electronic Structure of Graphene-Oxide. *Nano Lett.* **2009**, *9*, 1058–1063.
29. Lin, Y.; Zhou, B.; Martin, R. B.; Henbest, K. B.; Harruff, B. A.; Riggs, J. E.; Guo, Z. X.; Allard, L. F.; Sun, Y. P. Visible Luminescence of Carbon Nanotubes and Dependence on Functionalization. *J. Phys. Chem. B* **2005**, *109*, 14779–14782.